Journal of Biomedical Optics 5(4), 391–405 (October 2000)

Trans-abdominal monitoring of fetal arterial blood oxygenation using pulse oximetry

Anna Zourabian
Andy Siegel
Tufts University
Electro-Optics and Bioengineering Department
Medford, Massachusetts 02155

Britton Chance
Nirmala Ramanujan
University of Pennsylvania
Department of Biochemistry and Biophysics
Philadelphia, Pennsylvania 19104

Martha Rode
Hospital of the University of Pennsylvania
Philadelphia, Pennsylvania 19104

David A. Boas
Tufts University
Electro-Optics and Bioengineering Department
Medford, Massachusetts 02155
Massachusetts General Hospital
Department of Radiology
NMR Center
Charlestown, Massachusetts 02129

Abstract. Pulse oximetry (oxygen saturation monitoring) has markedly improved medical care in many fields, including anesthesiology, intensive care, and newborn intensive care. In obstetrics, fetal heart rate monitoring remains the standard for intrapartum assessment of fetal well being. Fetal oxygen saturation monitoring is a new technique currently under development. It is potentially superior to electronic fetal heart rate monitoring (cardiotocography) because it allows direct assessment of both the fetal oxygen status and fetal tissue perfusion. Here we present the analysis for determining the most optimal wavelength selection for pulse oximetry. The wavelengths we chose as the most optimal are the first in the range of 670–720 nm and the second in the range of 825–925 nm. Further, we discuss the possible systematic errors during our measurements and their contribution to the obtained saturation results. We present feasibility studies for fetal pulse oximetry, monitored noninvasively through the maternal abdomen. Our preliminary experiments show that the fetal pulse can be discriminated from the maternal pulse and thus, in principle, the fetal arterial oxygen saturation can be obtained. We present the methodology for obtaining these data, and discuss the dependence of our measurements on the fetal position with respect to the optode assembly.
 [S1083-3668(00)00604-3]

Keywords: fetal oxygen saturation; near infra-red spectroscopy; pulse oximetry; hemoglobin; optical properties.

Paper JBO-42023 received Dec. 29, 1999; revised manuscript received Apr. 13, 2000; accepted for publication June 26, 2000.

1 Introduction

Confirming the adequacy of oxygenation and ventilation is an integral part of monitoring the progress of critically ill patients. Although arterial blood gas (ABG) analysis has been the gold standard for early detection of arterial hypoxemia and hypercarbia, it is invasive, gives information only intermittently, and frequently imposes a substantial delay between sampling and the availability of results. To obtain a blood sample for ABGs a needle is placed in an artery. The radial artery is the usual source of the blood sample used for ABGs. This artery is close enough to the skin surface to be easily entered with a small needle. A blood sample is collected and run through an analyzer. Previous to oximetry this was the only way to assess a patient's oxygenation.

Pulse oximeters are examples of recent noninvasive blood gas monitors that have been widely used over the past two to three decades.[1,2] Pulse oximetry has many of the characteristics of an ideal monitoring technique: portability, noninvasiveness, and the capability for continuous on-line monitoring of arterial oxygen saturation (SaO_2). As a means of identifying hypoxia, it serves as another tool to give providers and physicians an insight into the patient's condition. In a sense, it acts as an early warning system. An individual's arterial oxygen saturation can fall well below 80% before clinical signs, such as cyanosis or a change in mental status, become evident.

Pulse oximeters take advantage of the fluctuations in the fraction of arterial blood in the tissue below the sensor. By monitoring the relative fluctuations from measurements at two wavelengths simultaneously, the arterial oxygen saturation is determined by making use of the differences between the absorption spectra of oxy- and deoxyhemoglobin. Pulse oximetry is now a standard for monitoring people during anesthesia and in critical-care situations. It is being applied for neonatal as well as for adult monitoring.

Currently electronic fetal heart rate monitoring is almost universally used as the standard for intrapartum assessment of fetal well being and is an indirect measure of fetal oxygenation and acid–base balance. However, the high false positive rate of this method has become a motivation for developing additional means for assessment of fetal well being. Such an addition to clinical assessment would, in turn, have the potential to influence clinical management in a manner that would decrease unnecessary fetal and maternal interventions. Currently, pulse oximetry devices to measure fetal oxygen saturation are under development as an adjunct to electronic fetal monitoring. Previous research by others has focused on *trans*-vaginal fetal pulse oximetry in which the sensor was placed on the fetal head or cheek.[3] This approach is only feasible

This paper was originally submitted to the April 2000 special issue honoring Britton Chance, but was not available in time.
Address all correspondence to Ms. Anna Zourabian, Massachusetts General Hospital, NMR Center, 13th St., Bldg. 149, Room 2301, Charlestown, MA 02129; E-mail: azoura01@emerald.tufts.edu

1083-3668/2000/$15.00 © 2000 SPIE

during labor and delivery. Also, small complications may occur near the sensor, such as bruises, indentations, or other irritations. Furthermore, uterine contractions increase the pressure of the sensor against the fetal scalp, leading to venous pulsations and therefore artifacts in the signal.[4] In addition, systematically low readings are obtained during delivery due to increases in scalp congestion, venous pulsations, and the accumulation of extracellular fluid.[4,5]

In the following, we present a brief introduction to fetal respiratory and circulatory physiology, and the background for oximetry and pulse oximetry. As an extension of the theoretical background of pulse oximetry, we present an optimal wavelength selection analysis, and discuss systematic errors caused by a number of assumptions made during this analysis. We demonstrate and evaluate the optical shunt problem (i.e., a fraction of the detected light exits the medium without reaching the fetus), which can potentially reduce the accuracy of our *trans*-abdominal measurements. Finally, we present our preliminary clinical results, and discuss areas of future research.

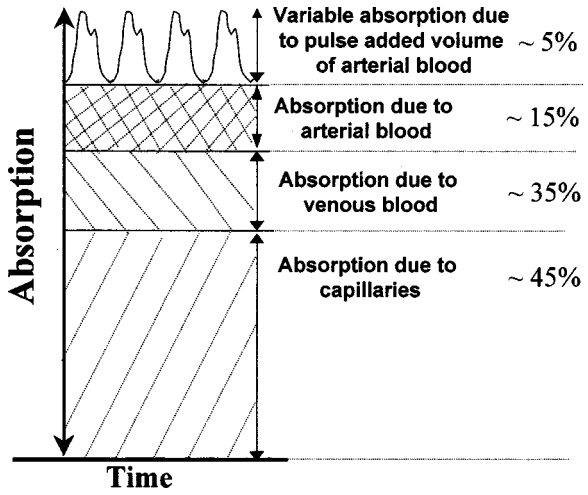

Fig. 1 Absorption of light by the arterial, venous, and arterial components of blood.

2 Pulse Oximetry

2.1 Background and Development

Pulse oximeters are widely used to monitor patient well being,[6–9] as they provide accurate information on arterial blood oxygen saturation. The advantage of pulse oximetry over oxygen tension monitors is that they provide a rapid response to changes in blood oxygenation and are noninvasive. The first oximeter used in a clinical environment was an ear oximeter, in which the transmission through the ear lobe was measured by a lamp and photocell attached to the ear.[6] (The terms ''oximetry'' and ''pulse oximetry'' represent different measurements: Pulse oximetry utilizes the pulsations of the arterial blood for extracting the oxygen saturation data, while oximetry does not.) This first oximeter did not utilize the pulsation of the arterial blood to extract oxygen saturation, but instead measured average hemoglobin oxygen saturation across vascular compartments. The mechanism is described as follows: the detected transmission in the red was related to changes in oxyhemoglobin and was compared to the transmission in green, which is relatively insensitive to changes in saturation. Subsequently, the red and green wavelength pair used for measuring the optical density of blood was replaced by 660 and 805 nm, where 805 was at the isosbestic point in the oxy- and deoxyhemoglobin spectra. The isosbestic point was chosen because the extinction coefficients of oxy- and deoxyhemoglobin are the same at that wavelength and therefore the optical density depends only on the total hemoglobin content. Oximetry often required heating the tissue in order to increase the blood flow to make it more representative of arterial blood. In order to calibrate for the effect of multiple scatter, the tissue was squeezed to temporarily remove the blood.

The evolution of the ear oximeters led to development of a pulse oximetry, which avoids the above mentioned inconveniences. Unlike regular transcutaneous oximetry described above, pulse oximetry is not based on an absolute measurement. It takes advantage of the pulsating nature of arterial blood, and the oxygen saturation values are obtained by taking the log ratio of the transmitted light at the highest and lowest points of the pulsation.

2.2 Pulse Oximetry

The light passing through the tissue exits with a slight amplitude modulation caused by pulsations of the arterial blood. The mathematical model for pulse oximetry is based on an arterial pulse-triggered measurement of the intensity of the light passing through the tissue. After each heart beat the arteries expand, increasing the volume fraction of blood and therefore increasing the absorption of light into the tissue. In other words the amount of light attenuated by the blood varies according to the pumping action of the heart. Figure 1 demonstrates the static absorption components in the tissue along with one dynamic component—the pulse-added volume of the arterial blood.

The advantage of pulse oximetry over absolute oximetry is that it avoids the need to make the tissue temporarily bloodless for calibration purposes. Instead it measures the light transmitted through the tissue at the high and low points of the pulse. The difference in the blood content of the tissue between those two points represents the modulation of the arterial blood volume. The logarithm ratio of the light transmitted at the low point to that transmitted at the peak (at both wavelengths) gives the optical densities necessary for oxygen saturation calculation.

2.3 Fetal Pulse Oximetry

Fetal pulse oximetry is a promising new technique currently under development for intrapartum monitoring, which gives information on both fetal heart rate and oxygen saturation. It is potentially superior to cardiotocography (CTG) because it permits direct assessment of the fetal oxygen status, which is likely to be a better indicator of fetal well being.

Previous research by others has focused on *trans*-vaginal fetal pulse oximetry in which the sensor was placed on the fetal head or cheek.[3–5,10] This approach is feasible during labor and delivery only. Small complications may occur near the sensor, such as bruises, indentations, or burns. Furthermore, uterine contractions increase the pressure of the sensor

against the fetal scalp, leading to venous pulsations and therefore artifacts in the signal.[4,5] In addition, systematically low readings are obtained during delivery due to increases in scalp congestion, venous pulsations, and the accumulation of extracellular fluid.[4,5,11,12] A *trans*-abdominal approach was applied[13] to measure fetal cerebral blood oxygenation *in utero* using near infra-red spectroscopy (NIRS). The major advantage of the *trans*-abdominal approach over the *trans*-vaginal is that the method is noninvasive to the mother and fetus, and the former approach can be used prior to labor as well as during labor. While preliminary evidence suggests that the noninvasive *trans*-abdominal method is sensitive to fetal oxygenation, the major problem with this approach is accurately and quantitatively discriminating the maternal and fetal contributions to the total detected signal.

We have developed an instrument for monitoring fetal oxygen saturation during the third trimester, noninvasively through the mother's abdomen. The light passing through the tissue will exit with a slight amplitude modulation caused by pulsatile flow in the arteries of both the mother and the fetus. The fetal pulse is discriminated from the maternal pulse by its different frequency. Hence, performing a Fourier transform on the detected signal allows us to separate the faster fetal signal from the slower maternal signals. The typical fetal heart rate lies between 1.5 and 2.5 Hz, while the material heart rate lies between 1 and 1.25 Hz.

3 Fetal Circulation

The fetal respiratory and circulatory system is significantly different from that of an adult. Arterial oxygen saturation in an adult is generally above 95%. In a normal fetus, on the other hand, the arterial oxygen saturation can be as low as 40%.[14] We briefly review fetal circulation to explain these differences and the implications for pulse oximetry.

The fetus gets its necessary nutrients via umbilical circulation in order to (a) build new tissues and increase its storage of substrates and (b) fuel energy metabolism. The transport of oxygen from the atmosphere to fetal tissues follows the following path: Oxygen is first transported into the maternal alveoli by respiration, and then it diffuses from the alveolar air into maternal blood. Maternal arterial blood pumped by the mother's heart transports oxygen from the lungs to the placenta. In the placenta, oxygen molecules diffuse from maternal to fetal blood. The highly oxygenated blood returning from the placenta to the fetus forms the blood that perfuses the fetal organs. Finally, the oxygen diffuses from the fetal blood to the cells of the fetal tissue. The transport of the CO_2 from fetal tissues to the atmosphere follows the same path in reverse.

Blood carrying oxygen and nutrients flows from the placenta to the fetus via the umbilical vein. Some of that highly oxygenated umbilical venous blood bypasses the liver and enters directly into the inferior vena cava (IVC) via the ductus venosus (see Figure 2). The remaining blood perfuses the liver. The blood from the IVC, now less oxygenated due to mixing of the placental and IVC blood, enters the right ventricle and is also shunted through the foramen ovale to the left ventricle. Most of the output from the right ventricle bypasses the lungs, and flows through the ductus arteriosus into the aorta. When entering the aorta, the blood from the ductus

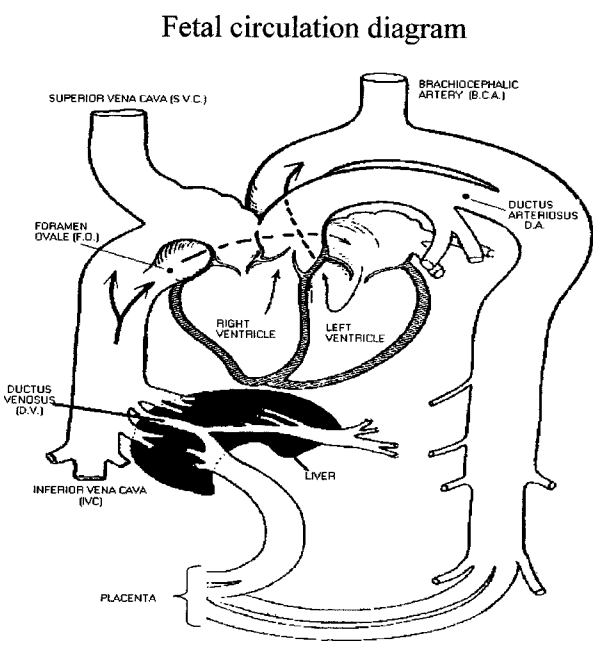

Fig. 2 Fetal circulation diagram.

arteriosus mixes with blood flowing from ascending to descending aorta to form the blood that perfuses the lower body and the placenta. The heart and the upper body are perfused exclusively by blood ejected from the left ventricle.

Umbilical cord gases indicate that fetal arterial oxygen saturation ranges from 40% to 70%.[14] These low values result because only a fraction of the blood is oxygenated in the placenta with each complete circulation through the body, as opposed to adults in which 100% of the blood is oxygenated with each circulation. It is thus necessary to take care in designing a fetal pulse oximeter to ensure that it is accurate at low saturation values.

4 Absorption and Scattering

Pulse oximetry measures the absorption of light by chromophores in the tissue. It measures changes in light transmission through, or back reflection from, a vascular bed, caused by an arterial blood volume increase with each ventricular contraction.

The absorption spectrum of an atom or molecule depends on its energy level structure, and thus provides a signature for identifying individual compounds. Measuring the concentration of an absorbing species in a sample is accomplished by applying the Beer–Lambert law. According to that law, the absorption of a sample at a given wavelength is directly proportional to the concentration of the absorbing material, its extinction coefficient, and the pathlength of light through it. The Beer–Lambert law assumes that the medium is homogeneous, the incident light is collimated, and reflection and scattering do not contribute to the loss of the transmitted light. The Beer–Lambert law is given by

$$\ln(I_0/I) = \sigma\rho d = \mu_a d \quad \text{or}$$
$$\log_{10}(I_0/I) = \epsilon C d = \frac{\mu_a d}{2.3} = \text{OD} = \text{absorbance}, \tag{1}$$

where I_0 is the incident intensity, I is the transmitted light intensity, σ is the absorption cross section, ρ is the number density of the absorbing molecules, C is the concentration of the absorbing molecules (in mM), d is the pathlength (in cm), ϵ is the extinction coefficient for a solution of molar concentration (in molar^{-1} cm^{-1}), and μ_a is the absorption coefficient (in cm^{-1}).

The Beer–Lambert law does not accurately describe the propagation of light through tissue; it has a number of limitations. Of most importance, the law, as written in Eq. (1), is in general valid for nonscattering media only. In addition it is valid for monochromatic light sources [although it is possible to modify this law to deal with nonmonochromatic sources (which will not be discussed here)], plus it does not hold true for substances exhibiting dichroism (i.e., substances that have different absorption spectra at different polarizations of light). These limitations are discussed in Ref. 15 and will not be discussed here.

The Beer–Lambert relation holds true when specular reflection or scattering does not contribute to the loss of transmitted light. This is clearly not the case in tissue. When the scattering length is shorter than or comparable to the absorption length, then the optical properties cannot be accurately determined using the Beer–Lambert law. The first attempts at diagnostic imaging using optical radiation revealed that multiple scattering, which occurs when visible to near-infrared light propagates through tissue, causes features below the surface to be blurred. As a consequence, measurement of the transmitted intensity through more than a few millimeters of tissue is dominated by scattered light. The characteristic scatter of tissues is commonly expressed in terms of the transport (or reduced) scattering coefficient (corresponding to isotropic scattering),

$$\mu_s' = \mu_s(1-g), \tag{2}$$

where μ_s is the scattering coefficient and g is the anisotropy factor of scattering equal to the average cosine of the single scattering phase function.[16]

In order to correct for the multiple scattering effect in the tissue we use the modified Beer–Lambert law,

$$\mathrm{OD} = -\log_{10}\frac{I}{I_0} = \sum_i \epsilon_i C_i L B + G. \tag{3}$$

B is a pathlength factor, which accounts for increases in the photon pathlength caused by tissue scattering and G is the measurement geometry factor, index ''i'' represents the ith chromophore. With each ventricular contraction, the arteries expand, increasing the volume fraction of blood and, therefore, increasing the absorption of light in the tissue. A change in the chromophore concentration causes the detected intensity to change. ϵ and L remain constant, and B and G are assumed to be constant. We therefore find that the change in optical density is given by

$$\Delta\mathrm{OD} = -\log_{10}\frac{I_{\mathrm{final}}}{I_{\mathrm{initial}}} = \sum_i \epsilon_i \Delta C_i L B. \tag{4}$$

By considering the contribution of only two chromophores, Hb and HbO, the above equation will look as follows:

$$\Delta\mathrm{OD}^{\lambda} = (\epsilon^{\lambda}_{\mathrm{HbO}}\Delta[\mathrm{HbO}] + \epsilon^{\lambda}_{\mathrm{Hb}}\Delta[\mathrm{Hb}])LB^{\lambda}. \tag{5}$$

This equation accounts for independent concentration changes in oxy- and deoxyhemoglobin. The changes in oxy- and deoxy-Hb concentrations (and therefore the change in total Hb concentration) are assumed to be wavelength independent. This assumption could be invalid if different wavelengths sample different volumes of tissue with different hemoglobin concentrations. The quantity of oxygen in the blood is often expressed as the hemoglobin oxygen saturation (S), which is defined as

$$S = \frac{[\mathrm{HbO}]}{[\mathrm{HbO}]+[\mathrm{Hb}]}\times 100 = \frac{[\mathrm{HbO}]}{[\mathrm{HbT}]}\times 100 \quad (\%). \tag{6}$$

This expresses the percentage of the total oxygenated hemoglobin.

By taking the ratio (R) of the changes in optical density measured at two different wavelengths we get the following expression:

$$R = \frac{\Delta\mathrm{OD}^{\lambda_1}}{\Delta\mathrm{OD}^{\lambda_2}} = \frac{[\epsilon^{\lambda_1}_{\mathrm{HbO}}S + \epsilon^{\lambda_1}_{\mathrm{Hb}}(1-S)]\Delta[\mathrm{HbT}]LB^{\lambda_1}}{[\epsilon^{\lambda_2}_{\mathrm{HbO}}S + \epsilon^{\lambda_2}_{\mathrm{Hb}}(1-S)]\Delta[\mathrm{HbT}]LB^{\lambda_2}}. \tag{7}$$

By solving for hemoglobin oxygen saturation (S), we obtain the following final expression:

$$S = \frac{\epsilon^{\lambda_2}_{\mathrm{Hb}}R(B^{\lambda_2}/B^{\lambda_1}) - \epsilon^{\lambda_1}_{\mathrm{Hb}}}{(\epsilon^{\lambda_1}_{\mathrm{HbO}} - \epsilon^{\lambda_1}_{\mathrm{Hb}}) - R(B^{\lambda_2}/B^{\lambda_1})(\epsilon^{\lambda_2}_{\mathrm{HbO}} - \epsilon^{\lambda_2}_{\mathrm{Hb}})}. \tag{8}$$

The B factor can be estimated by solving the photon diffusion equation for the appropriate measurement geometry. For a semi-infinite homogeneous medium, one finds that (Boas et al., unpublished data)

$$B = \frac{1}{2}\left(\frac{3\mu_s'}{\mu_a^{\mathrm{initial}}}\right)^{1/2}\left(1 - \frac{1}{1+L(3\mu_s'^{\mathrm{initial}}\mu_a^{\mathrm{initial}})^{1/2}}\right). \tag{9}$$

This shows that the pathlength factor depends on the absorption, and therefore on the extinction coefficient, and therefore is wavelength dependent. In practical clinical measurements this dependence is ignored, and the B parameter is determined empirically. Equation (9) also shows that the pathlength factor depends on the optode separation and on the tissue scattering.

In summary, Eq. (8) shows that if we measure the changes in optical density (caused by arterial pulsations) at two different wavelengths, and if the molar extinction coefficients of the oxy- and deoxyhemoglobin are known, then we can easily calculate the arterial oxygen saturation.

5 Wavelength Selection

5.1 Wavelength Selection Background

One of the first oximeters, built in 1935,[17] had only one wavelength, which was located in the red region of the spectrum. Using only one wavelength prevented it from compensating for changes in hemoglobin concentration. Matthes[18] overcame

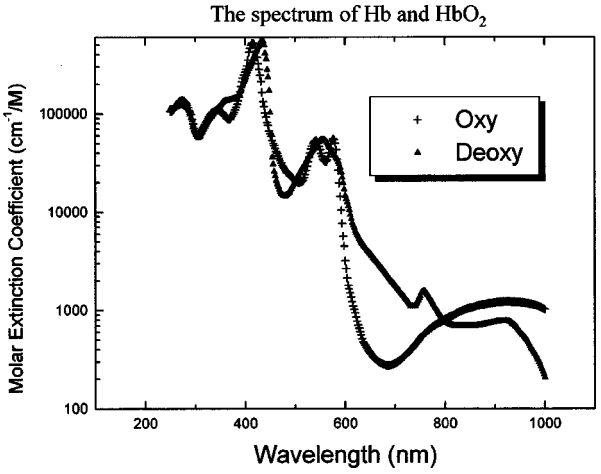

Fig. 3 Oxy- and deoxyhemoglobin spectrum. The absorption coefficient (in units of cm^{-1}) is given by $\mu_a = 2.3\,(\epsilon_{HbO}[HbO] + \epsilon_{Hb}[Hb])$, where [HbO] and [Hb] are the molar concentrations of oxy- and deoxyhemoglobin.

this problem by using two wavelengths (one red and one green). The green wavelength was soon replaced by an infrared wavelength[19] because the absorption of the blood in the green region was so great that the light could only be transmitted through very thin layers of tissue. The resulting oximeter used one red wavelength (usually around 660 nm) as a measure of the oxyhemoglobin, and one infrared as a reference (~805 nm). The latter is a wavelength at which the extinction coefficients of both oxy- and deoxyhemoglobin are the same (the isosbestic point), and therefore the optical density depends on the total hemoglobin concentration and not on the oxygen saturation. This reduces the expression for oxygen saturation to $SaO_2 = a + b(OD^{\lambda_1}/OD^{\lambda_2})$, where the constants a and b are empirically determined. In pulse oximeters currently used in hospitals, usually one of the wavelengths is at the isosbestic point.

Given the wavelength dependence of the measurements, we are confronted with the question, Which wavelengths provide the best saturation sensitivity? In other words, we want to choose a pair of wavelengths that will give us the minimum error in our calculations and maximum sensitivity to changes in oxygen saturation across a broad range of saturations. This problem was discussed by Mannheimer et al. in 1997.[20] Their numerical modeling suggested that 735 and 890 nm emitters should provide better accuracy at low saturation than sensors made with conventionally used 660 and 900 nm emitters. Later, in 1999, Smith[21] suggested a combination of 635 and 905 nm wavelengths to improve oxygen sensitivity.

5.2 Wavelength Selection Analysis

As we can see from Eqs. (7) and (8), the saturation depends on the molar extinction coefficients, which in turn are wavelength dependent. The dependence of the molar extinction coefficients of the oxy- and deoxyhemoglobin are shown in Figure 3.

The error in oxygen saturation σ_S is calculated as

$$\sigma_S = \frac{\partial S}{\partial R}\sigma_R = \frac{(\epsilon_{Hb}^{\lambda_2}\epsilon_{HbO}^{\lambda_1} - \epsilon_{HbO}^{\lambda_2}\epsilon_{Hb}^{\lambda_1})(B^{\lambda_2}/B^{\lambda_1})}{[\epsilon_{HbO}^{\lambda_1} - \epsilon_{Hb}^{\lambda_1} - R(B^{\lambda_2}/B^{\lambda_1})(\epsilon_{HbO}^{\lambda_2} - \epsilon_{Hb}^{\lambda_2})]^2}\sigma_R, \tag{10}$$

where σ_R, the error in R, is the ratio of the optical densities at two different wavelengths, which is given by

$$\frac{\sigma_R}{R} = \left[\left(\frac{\sigma_{\Delta OD^{\lambda_1}}}{\Delta OD^{\lambda_1}}\right)^2 + \left(\frac{\sigma_{\Delta OD^{\lambda_2}}}{\Delta OD^{\lambda_2}}\right)^2\right]^{1/2}, \tag{11}$$

where $\sigma_{\Delta OD^{\lambda_1}}$ and $\sigma_{\Delta OD^{\lambda_2}}$ are the errors in the optical densities at two different wavelengths. The change in optical density is given by

$$\Delta OD = (\epsilon_{HbO}\Delta[HbO] + \epsilon_{Hb}\Delta[Hb])LB. \tag{12}$$

By combining Eq. (9) in Sec. 4 and Eq. (12) we obtain, for a measurement made on the surface of a semi-infinite medium,

$$\Delta OD = \frac{1}{2}\sqrt{\frac{3\mu_S'}{\mu_a}}\left(1 - \frac{1}{1 + L\sqrt{3\mu_S'\mu_a}}\right) \times (\epsilon_{HbO}\Delta[HbO] + \epsilon_{Hb}\Delta[Hb])L, \tag{13}$$

where

$$\mu_a = 2.3(\epsilon_{HbO}[HbO] + \epsilon_{Hb}[Hb]). \tag{14}$$

By plotting Eq. (10) versus wavelength we are able to visualize the wavelength dependence of the saturation error. The resulting dependence is illustrated in Figure 4(a). The image shown is symmetrical around the diagonal axis and was calculated using the following baseline conditions: $\mu_S' = 10\ cm^{-1}$, $[HbO]_{initial} = 0.85\ \mu M$, $[Hb]_{initial} = 0.15\ \mu M$, a 10% modulation (pulse added volume of oxy- and deoxyhemoglobin), and $L = 1$ cm. We assumed a constant 1% measurement error at both wavelengths, i.e., $\sigma_{OD} = 1\%$ independent of wavelength.

Figure 4 demonstrates the dependence of the saturation error on the wavelengths over the range of 600–1000 m. The image is displayed on a $\log_{10}$ scale. The darker blue areas indicate a lower saturation error, which increases as the color turns to red.

According to the plot, in order to obtain the minimum saturation error, one of the two wavelengths needs to be in the range of 650–720 nm and the second wavelength in the 850–1000 nm range. Decreasing the oxygen saturation from 85% to 45% does not change the optimal wavelengths, nor does it have a significant effect on the saturation error.

In this approach we assumed that the measurement error remained constant and was independent of wavelength. Smith made the same assumptions in Ref. 21 and obtained the same result. This assumption is invalid. In general, the detected signal and its measurement error can change significantly with wavelength due to absorption in the tissue. In Sec. 5.3 we derive the wavelength dependence of the measurement error, and implement that result into the saturation error calculation.

5.3 Systematic Errors

The assumptions made in the process of the calculation and analysis of the saturation error are

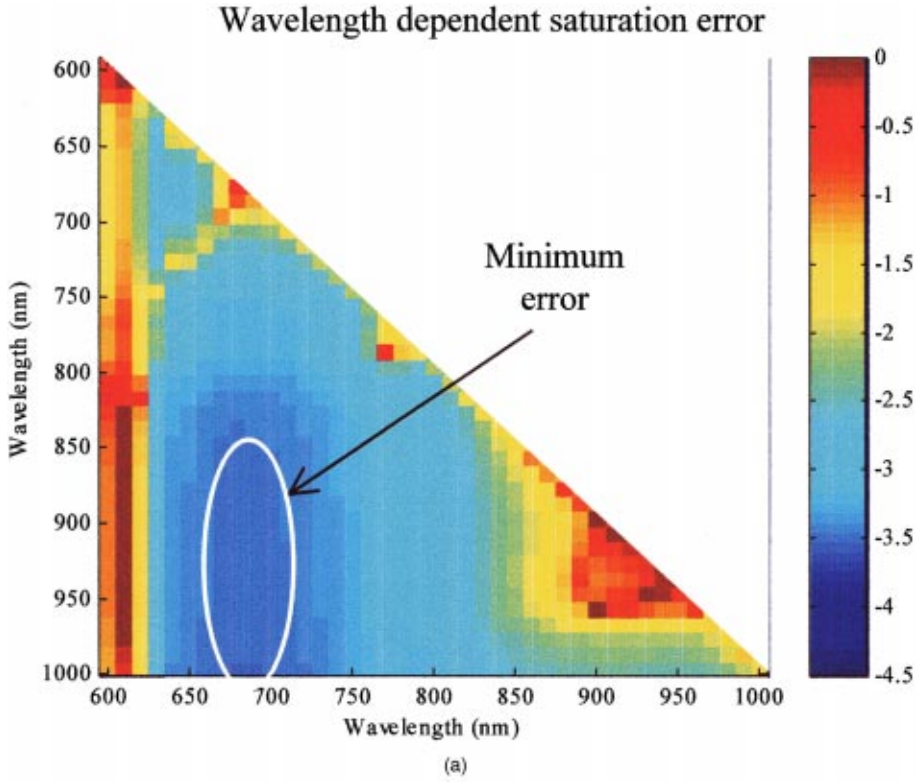

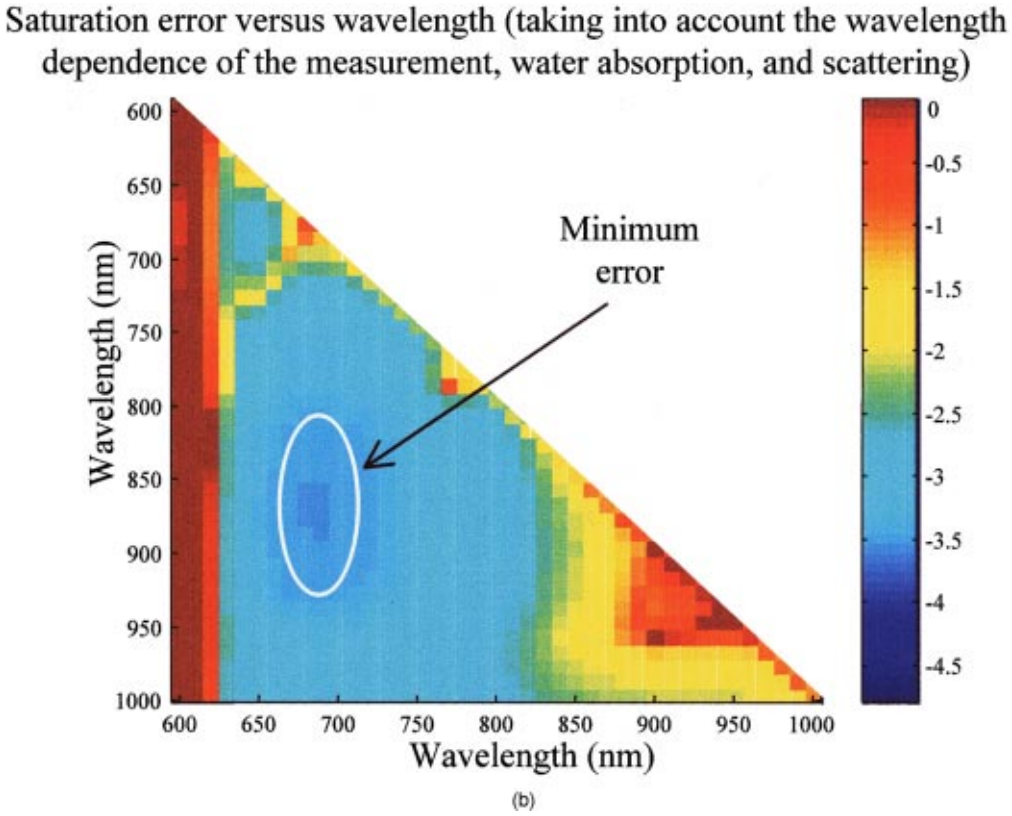

Fig. 4 (a) Image of the wavelength dependent saturation error. The color scale is $\log_{10}$ such that the minimum error is $\sim 10^{-3.5}$. The error for wavelengths of 600 and 650 nm is only slightly larger than the optimal wavelength pair of 670 and 925 nm. (b) Saturation error vs wavelength (taking into account the wavelength dependence of the measurement error on hemoglobin absorption, water absorption, and scattering). The color scale is $\log_{10}$ such that the minimum error is $\sim 10^{-3.5}$.

- Hb and HbO are the only absorbing chromophores present in tissue;
- scattering is independent of wavelength;
- we assumed a constant 1% error in the measurement ($\sigma_{\Delta OD}$).

There are a number of other chromophores present in the tissue: cytochromes, lipids, haemiglobin (Hi) (also called methemoglobin), carboxyhemoglobin (HbCO), etc. Lipids do not significantly add to the overall extinction coefficient of the tissue, since lipids are only present at roughly one-tenth proportion compared to water. Typical concentrations of HbCO are less than 10% of the total hemoglobin content; in addition, the near-infrared effect of the HbCO is negligible because of its low extinction coefficients in that spectral region. Neglecting the effect of haemiglobin, on the other hand, could potentially introduce larger errors in the measurements. However, haemiglobin's tissue concentration is low with respect to the total hemoglobin concentrations. Ignoring the contribution of the Hi may introduce error, which can reach 1% of the total hemoglobin signal.[15]

Regarding the second assumption, it is a well known fact that light absorption of the compounds present in the human tissue greatly depend on the wavelength of the incoming radiation. The scattering dependence on the wavelength, on the other hand, is neglected in most of the cases. In human dermis, scattering dominates over absorption. The forward directed scattering is believed to be due to collagen fibers.[22] Experimental observations reveal that the reduced scattering coefficient decreases with increasing wavelength as $\mu_s' \sim \lambda^{-1.5}$ (private communication with S. L. Jacques). This dependence is incorporated into our calculation of the wavelength dependent error in ΔOD.

The ΔOD is calculated from the measured intensities: $\Delta OD = -\log_{10}(\Phi_{final}/\Phi_{initial})$ (the fluence is directly proportional to the intensity). Therefore the absolute error in the change of the optical density is

$$\sigma_{\Delta OD} = \frac{\partial \Delta OD}{\partial \Phi}\sigma_{\Phi}. \tag{15}$$

The absolute photometric error is σ_Φ (which we assumed initially to be constant versus wavelength and saturation). σ_Φ arises from the root-sum-square combination of shot noise and electronic noise,

$$\sigma_{\Phi} = (\sigma^2_{electronic} + \sigma^2_{shot})^{1/2}. \tag{16}$$

5.3.1 *Electronic noise*

Electronic noise is introduced when the signals are generated, amplified, and typically fed through an analog-to-digital converter. This noise is assumed to be independent of exposure time and independent of wavelength, and to depend only on the electronics of the circuit and is thus assumed constant throughout the experiment.

5.3.2 *Shot noise*

Shot noise occurs at low flux levels, when the signal to noise ratio (S/N) is limited by the shot noise produced by the optical power itself. Since the noise is a function of the square root of the incoming signal power [$P(t)$], the S/N only increases as the square root of the signal power. A signal carried by N photons will have $\sigma_{shot} = \sqrt{N}$ photons of shot noise. A certain fraction of the detected photons, determined by its quantum efficiency, is detected and the electrons produced by these photons are then read out. The photon rate (photons per second) can be calculated using the following expression:

$$r = P(t)/h\nu = \lambda P(t)/1.24, \tag{17}$$

where $h\nu(eV) = h\nu/q = hc/q\lambda = 1.24/\lambda(\mu m)$. The signal traveling through the tissue carried by Φ, the photon fluence, will have $\sigma_{shot} = \sqrt{\Phi}$ shot noise. Using the solution to the diffusion equation for semi-infinite media,[23] we find

$$\Phi = \frac{cS}{4\pi D}\left[\frac{\exp(-\sqrt{3\mu_s'\mu_a}r_1)}{r_1} - \frac{\exp(-\sqrt{3\mu_s'\mu_a}r_2)}{r_2}\right], \tag{18}$$

where c is the speed of light in the medium, D is the photon diffusion coefficient given as $D = c/3\mu_s'$, and S is the source term with units of power. r_1 and r_2 are given as follows: $r_1 = \sqrt{L^2 + (z_0 - z_S)^2}$, $r_2 = \sqrt{L^2 + (z_0 + 2z_b + z_S)^2}$, where z_S is the position where the collimated light source (perpendicular to the surface) becomes diffuse inside the medium, z_i is the position of the image source used to satisfy the semi-infinite boundary condition, z_b is the position of the extrapolated boundary, and L is the displacement between the collimated light source and the detector.

The source term in Eq. (18) can be written as $\lambda P(t)/1.24$ [see Eq. (17)]. We thus obtain an explicit equation for the wavelength dependence of the shot-noise as

$$\sigma_{shot} = \left[\frac{c\lambda P}{4.96\pi D}\left(\frac{\exp(-\sqrt{3\mu_s'\mu_a}r_1)}{r_1} - \frac{\exp(-\sqrt{3\mu_s'\mu_a}r_2)}{r_2}\right)\right]^{1/2}. \tag{19}$$

By combining the electronic noise and shot noise terms we obtain an expression for the absolute error in our measurement [see Eq. (16)]. The main goal of this analysis was to determine how our measurement error depends on the wavelength. Since the electronic noise power is independent of the wavelength, it was assumed constant for the purpose of our analysis. Assuming that $\sigma_{electronic} \ll \sigma_{shot}$, we obtain the following expression for the measurement error:

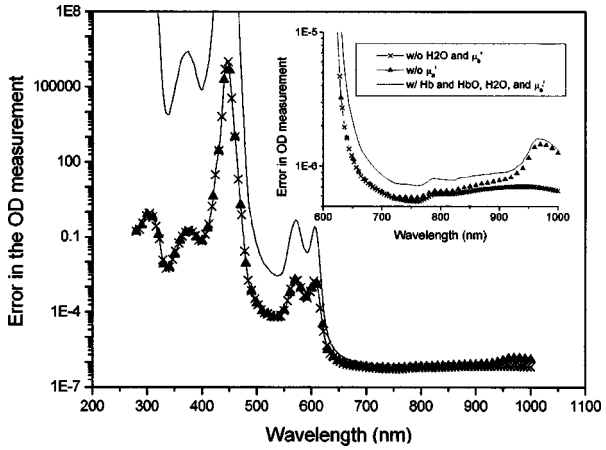

Fig. 5 Wavelength dependence of the measurement error considering the independent wavelength contributions from hemoglobin, water, and scattering.

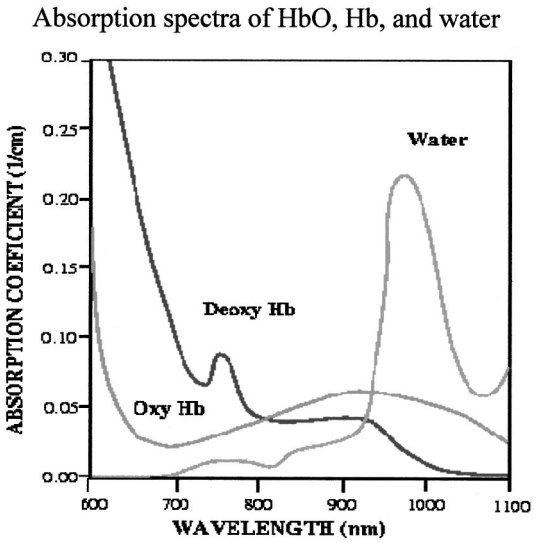

Fig. 6 Absorption spectra of HbO, Hb, and water. The absorption coefficient is given for 5% whole blood (typical tissue concentration) and 100% water.

$$\sigma_{\Delta OD} = \frac{1}{[(\nu\lambda P/4.96\pi D)(\exp(-\sqrt{3\mu_s'\mu_a}r_1)/r_1 - \exp(-\sqrt{3\mu_s'\mu_a}r_2)/r_2)]^{1/2}}. \quad (20)$$

5.4 Wavelength Dependence of the Measurement

The plot showing the dependence of the measurement error ($\sigma_{\Delta OD}$) on the wavelength, i.e., the expression given by Eq. (20), is shown in Figure 5. The three curves correspond to, respectively, (1) error in the measurement without taking into account the water absorption and scattering effects, (2) taking into account the water absorption but not the scattering effect, (3) taking into account both water absorption (along with hemoglobin absorption), and the scattering effect. The average water content in the human body is approximately 65%, therefore the absorption properties of water affect our measurements. The first and second curves (with and without water absorption) look almost identical because at wavelengths below 850 nm, absorption by water is orders of magnitude lower than the absorption by hemoglobin and therefore its contribution is insignificant. The absorption of water increases at wavelengths above 900 nm, and correspondingly the optical signal decreases. The visible and near-infrared spectrum of water is presented in Figure 6,[24] along with the spectra of oxy- and deoxyhemoglobin. The third curve shows the expected result that the stronger scattering at shorter wavelengths has a more pronounced effect on the measurement error.

Figure 5 demonstrates that the measurement error does indeed depend on the wavelength. This is not surprising, since we know that the measured signal depends on absorption and scattering by the components in the tissue. In the regions with higher absorption we get higher sensitivity, but with low S/N levels. A stronger signal can be achieved in the 650–900 nm range, where the absorption is still strong enough to provide sensitivity at higher S/N levels.

The measurement error in the previous wavelength selection simulations was assumed constant at 1%, and independent of wavelength. In previous publications it was also assumed that the measurement error remains constant over different wavelengths.[21] Now, by implementing the wavelength dependence of the measurement, the wavelength dependence of the scattering, and the effect of the water absorption into the saturation error analysis we obtain the results illustrated in Figure 4(b). This dependence was calculated for 5% whole blood contained in soft tissue, 85% oxygenated hemoglobin, 15% deoxyhemoglobin, and 10% change in total hemoglobin concentration caused by arterial pulsations. Decreasing the oxygen saturation from 85% to 45% does not change the optimal wavelengths, but does increase the saturation error by approximately a factor of 10.

The simulations and analysis described in this paper, the goal of which was to choose a pair of wavelengths allowing minimum error in oxygen saturation calculations along with maximum signal strength, led us to choose the following wavelengths for pulse oximetry: 670–700 and 850–890 nm. This is opposed to 660–710 and 850–1000 nm determined when neglecting the wavelength dependent measurement error. Furthermore, the obtained results are different from the results published by Mannheimer et al.[20] and by Smith.[21] The major difference between our approach and the approach suggested by Mannheimer et al. is that they derive their optimal wavelength pair by taking into account the changes in blood volume and choosing wavelengths with closely matching penetration depths. Smith's analysis, on the other hand, is very similar to our approach with one major difference: He assumed the absolute measurement error to be constant across wavelength and saturation values, which, as we demonstrated in Figure 5, is not true. The trade-off between the systematic errors of differing depth penetration (minimized by Mannheimer et al.) and the measurement noise (minimized by Smith and us) needs further analysis with real experimental data.

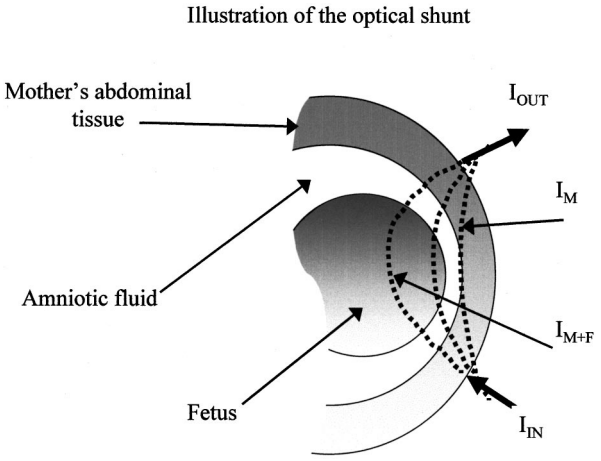

Fig. 7 Illustration of the optical shunt problem (see the text for details).

6 Optical Shunt Problem

6.1 Illustration of the Problem

For fetal pulse oximetry, our approach is to monitor fetal arterial blood oxygenation through the mother's abdomen. This means that the optical radiation from the sources must travel through the mother's tissue, pass through the amniotic fluid separating the fetus from the mother, reach the fetus, and then travel back to a detector located on the mother's abdomen. The detected signal contains information about (1) mother only—when the source–detector separation is small, and the ''banana pattern'' covers only the maternal tissue and (2) mother and the fetus—when the source–detector separation is large enough for sufficient light penetration to ''see'' the fetus. The maternal and fetal contributions to the modulation of the incoming light caused by the pulsations of the arterial blood of the two can be easily separated because they appear as separate peaks in the Fourier transform. But the calculation of the oxygen saturation of the modulated signal requires normalization to the dc level of the detected signal, which in our case combines the dc levels from both mother and fetus. As the task of separating the dc levels of two signals (maternal and fetal) is extremely difficult, if not impossible, we must either assume a value for the maternal contribution to the dc level or neglect it. Here in Sec. 6 we investigate the effect that this assumption has on our measurements.

Figure 7 illustrates the problem described above. The darker outer circle represents a cross section of the maternal abdomen, the lighter one represents that of the amniotic fluid, and the smallest dark circle represents the fetal body. As shown in Figure 7, the incident light samples different parts of the medium, and the exiting intensity is the combination of that light which has traveled through the fetal+maternal tissue and amniotic fluid (I_{F+M}), as well as that light, which has traveled only through the maternal abdominal tissue and the amniotic fluid only (I_M).

As was mentioned earlier, the change in optical density can be calculated by

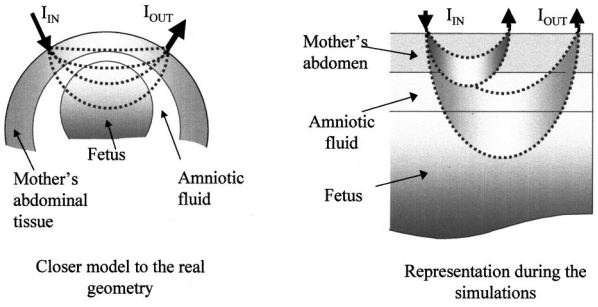

Fig. 8 Real and simulation geometry representations.

$$\Delta \mathrm{OD} = -\log_{10}\frac{I_{\max}}{I_{\min}} = (\epsilon_{\mathrm{HbO}}\Delta[\mathrm{HbO}] + \epsilon_{\mathrm{Hb}}\Delta[\mathrm{Hb}])LB. \tag{21}$$

$I_{\max}$ and $I_{\min}$ are the intensities detected at the surface of the maternal tissue corresponding to the maximum and minimum light intensity, respectively, caused by the arterial pulsation. This exiting intensity contains both maternal and fetal signals, i.e., $I_{\max}=I_{M+F}+I_M$. If we do not know or do not wish to assume the dc value of I_M, we must then neglect it and thus assume that

$$(I_M+I_{M+F})/I_{\min}=I_{M+F}/I_{\min}. \tag{22}$$

Our task is to determine the systematic error introduced by this assumption.

In this calculation we also assume that the light detected at different wavelengths has been exposed to equal portions of fetal modulated blood. This assumption could be true for transmission oximetry, but in our case where we analyze backreflected light, two different wavelengths do not necessarily penetrate to the same depths inside the tissue. A possible solution is to choose wavelengths with penetration depths as close to each other as possible. This solution is problematic because, as the oxygen saturation in the blood changes, the wavelength dependent penetration depth also changes.[20] To compensate for this we could use two different wavelength pairs for high and low oxygen saturation cases.

6.2 Simulations

In order to quantify the magnitude of the optical shunt we performed a series of simulations. During the simulations the maternal abdominal tissue, the fetal body, and the amniotic fluid separating the two were represented as planar layers in (x,y,z) coordinates. An example of the typical simulation geometry is illustrated in Figure 8.

Scattering and absorption coefficient values were assigned to each of the layers. Simulations were performed for different thicknesses of the maternal and amniotic fluid layers. The fetal layer was kept semi-infinite for all the simulations. We used the Monte Carlo method for simulating the *trans*-abdominal measurements.[25] In this method the histories of individual photons are simulated as they undergo scattering and absorption events in the medium. Each photon is followed until it disappears (gets absorbed or has a negligible contribution) or escapes the surface of the medium and therefore gets detected. In other words, the Monte Carlo method simulates

Table 1 Detected signal values for the two simulation cases.

Case No. 1. Fetal layer with very high absorption			
S/D separation (mm)	25	50	75
Detected signal I_M	1.51 *e*3	2.89 *e*1	5.12 *e*1
Case No. 2. Optical properties of both layers are close to reality			
Detected signal $I_{M+F}+I_M$	1.58 *e*3	8.2 *e*1	3.63 *e*1
Difference in intensities detected for Case Nos. 1 and 2			
I_{M+F} $(I_{M+F}-I_M)$	0.07 *e*3	5.31 *e*1	3.57 *e*1

Table 2 Fraction of the total detected signal in each layer.

S/D separation (mm)	25	50	75
Total detected signal	1.58 *e*3	8.2 *e*1	3.63 *e*1
Fraction of light in the maternal layer I_M^{frac}	0.95	0.35	0.014
Fraction of light in the fetal layer I_F^{frac}	0.05	0.65	0.986

the ''random walk'' of the photons in the medium perturbed by spatially varying absorption and scattering properties. The rules of photon propagation are given as probability distributions for the incremental steps of photon movement within the medium. One million photons were used in our simulation.

6.3 Simulation Results

Simulations were made for two different cases. The two simulations were

- the maternal and amniotic layers were assigned realistic optical parameters, and the fetal layer was given an infinitely high absorption;
- the maternal, amniotic, and fetal layers were all given realistic optical properties.

The first simulation was performed to find the maternal signal only. The signal from the first simulation subtracted from that of the second simulation gives the fetal contribution to the total signal. The maternal layer thickness for both cases was 1 cm, the thickness of the amniotic fluid was also kept constant for both simulations and was 1 cm, and the fetal layer thickness was infinite. Optical properties of the layers were chosen as follows: $\mu_{a(\text{mother})}=0.05\ \text{cm}^{-1}$; $\mu_{a(\text{amniotic})}=0.012\ \text{cm}^{-1}$; $\mu_{a(\text{fetus})}=0.15\ \text{cm}^{-1}$. The reduced scattering coefficient was the same for both maternal and fetal layers, and was $10\ \text{cm}^{-1}$. For the amniotic fluid, $\mu_S'=0.1\ \text{cm}^{-1}$. These values may be somewhat arbitrary, however, the conclusions drawn from these simulations hold for a wide range of parameter values. For both simulations there was a light source on the surface of the mother's abdomen, and the backscattered light was measured for different separations from the source. The simulation also provided information on the sensitivity of the detected signal to each layer of the medium. The sensitivity is a measure of how much the detected signal changes with absorption changes in each particular layer.

Table 1 indicates the detected signal at three different source/detector separations for two simulations. For the first case the simulation corresponds to the ''maternal'' signal only (I_M), since any light reaching the fetal layer would be absorbed and would not contribute to the output signal. The detected signal for the second case is the combination of both fetal and maternal signals ($I_{M+F}+I_M$). By subtracting the result of the first simulation from that of the second simulation, we obtain the amount of light that sampled the fetal layer, which we denote as I_{M+F}.

Table 2 shows the fraction of the total detected signal (for three different source/detector separations) that reaches each layer. The fraction of light in the maternal layer represents the shunt signal. We see that the shunt signal dominates at the 25 mm source/detector separation. At 50 mm separation, 35% of the total detected signal passes through the maternal and amniotic layers without reaching the fetal layer, and 65% of it reaches the fetus. At separation of 75 mm the shunting signal is only 1.4%.

How does the shunt affect the accuracy of the fetal oxygen saturation measurement? As was shown earlier, in order to obtain the oxygen saturation we need to measure the change in optical density due to arterial pulsations. The change in optical density is given as the log of the ratio of the transmitted intensity amplitudes of the pulsatile (ac) component to the nonpulsatile (dc) component. Suppose there is 5% modulation in the absorption coefficient of the fetal layer (i.e., $\Delta\mu_{a(\text{fetal})}/\mu_{a(\text{fetal})}=5\%$), caused by fetal arterial pulsations. Then the fraction of the fluctuations of the total output signal caused by the arterial pulsations of the fetal layer only can be calculated as

$$\left(\frac{\partial I_{\text{total}}}{\partial \mu_{a,\text{fetal}}}\right)\frac{1}{I_{\text{total}}}\Delta\mu_{\text{fetal}}=\frac{\partial I_{\text{M+F}}}{\partial \mu_{a,\text{fetal}}}\frac{\Delta\mu_{a,\text{fetal}}}{I_{\text{total}}}=\frac{\Delta I_{\text{M+F}}}{I_{\text{total}}}, \tag{23}$$

where I_{total} is the total signal detected at the surface of the medium, and $\Delta I_{\text{M+F}}$ is the fraction of the total output signal modulation caused by absorption modulations in the fetal layer. The change in optical density that we actually measure is given as

$$\begin{aligned}\Delta\text{OD}_{\text{meas}}&=-\log_{10}\frac{I_{\text{total}}+\Delta I_{\text{M+F}}}{I_{\text{total}}}\\&=-\log_{10}\left(1+\frac{\Delta I_{\text{M+F}}}{I_{\text{total}}}\right)\approx\frac{\Delta I_{\text{M+F}}}{I_{\text{total}}}.\end{aligned} \tag{24}$$

What we really want to measure is the change in optical density corrected to remove the shunt signal,

Table 3 Fractional errors between the measured value of the optical density and the desired OD, along with the fractional error between the saturation values calculated using measured and desired values of the optical densities.

Optode separation (mm)	Fractional error in OD [Eq. (26)]		Fractional error in saturation (%)
	at 700 nm (%)	at 900 nm (%)	
25	26	36	5.00
50	4	4	0.46
75	3	4	1.40
100	3	4	1.00

$$\Delta \mathrm{OD}_{\mathrm{real}} = -\log_{10}\frac{I_{\mathrm{M+F}}+\Delta I_{\mathrm{M+F}}}{I_{\mathrm{M+F}}} = -\log_{10}\left(1+\frac{\Delta I_{\mathrm{M+F}}}{I_{\mathrm{M+F}}}\right) \approx \frac{\Delta I_{\mathrm{M+F}}}{I_{\mathrm{M+F}}}. \quad (25)$$

The fractional error between the measured and real values of the optical densities is

$$\text{fractional error} = \frac{\Delta \mathrm{OD}_{\mathrm{meas}} - \Delta \mathrm{OD}_{\mathrm{real}}}{\Delta \mathrm{OD}_{\mathrm{real}}} = \frac{I_{\mathrm{M+F}}}{I_{\mathrm{total}}} - 1. \quad (26)$$

To obtain the oxygen saturation, a measurement at two different wavelengths is necessary. In Table 3, we show the fractional errors resulting from measurements made at 700 and 900 nm with a fetal and maternal oxygen saturation of 85%. The total hemoglobin concentration for the fetus (mother's abdominal tissue) was assumed to be 0.1 mM (0.025 mM). The reduced scattering coefficient was held constant at 10 cm^{-1}. From Table 3 we see that the fractional errors between the measured value of the optical density and the desired OD can be quite large (>20%), but they are nearly the same at the two different wavelengths. For the saturation calculation we use relative measurements at two different wavelengths. The third column in Table 3 shows the fractional error between the saturation values calculated using measured and desired values of the optical densities. These results indicate that, when the systematic errors at the two wavelengths caused by the optical shunt are nearly the same, then the ratio tends to reduce (or cancel) the error, resulting in a relatively more accurate value for the oxygen saturation. Note, however, that for our analysis we used a simplified model of layered media. Measurements on human subjects are expected to contain additional noise components both of instrumental and biological nature. A similar error analysis for diffuse optical tomography can be found in Ref. 26, where Cheng et al. show that even though the error in an absolute measurement at one wavelength can be significant, the error in a relative measurement at two different wavelengths can be acceptable.

In conclusion, although at one wavelength the error in the OD due to the optical shunt can be significant (especially at the smaller separations, where the shunt is larger), a relative measurement at two different wavelengths significantly reduces the systematic error to a more acceptable level.

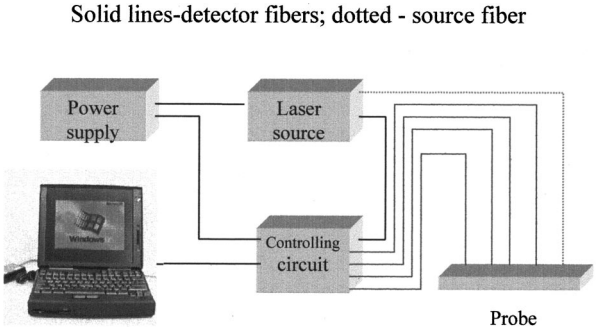

Fig. 9 Optical fetal monitor block diagram (described in the text).

7 Clinical Study

The goal of our pilot clinical study was to indicate feasibility for obtaining fetal arterial oxygen saturation values noninvasively, through the mother's abdomen. Briefly, the subject population was that selected for the nonstress test (NST), which measured fetal heart rate accelerations associated with spontaneous fetal movements *in utero*. Initially, all women undergoing NST were eligible for this test. This study was reviewed and approved by the Institutional Review Boards of the University of Pennsylvania and written consent was obtained from all patients that participated. In addition to the ultrasound transducer and tocodynamometer employed in the NST test, our optical sensors were attached on either side of the patient's abdomen, with a light source on one side of the abdomen and the detector on the other side of the abdomen to afford light transmission through the uterus and fetus. Measurements were only obtained at a single wavelength to simply demonstrate that the fetal pulse modulation of the optical signal can be discriminated from the maternal signal.

7.1 Single Wavelength Instrument

The optical fetal monitor unit (illustrated in Figure 9) consists of five modules: the system power supply; the laser source; the control module; the optode assembly; and the computer. The laser source generates the optical signal, which reaches the optode assembly through a 1 mm diam silica fiber. Its output is modulated at a fixed frequency of 2 kHz to permit synchronous detection.

The system presently consists of a single wavelength light source and four separate optical detectors. The detectors, each spaced 1 in. (2.5 cm) apart on the optode assembly (Figure 10), are coupled to the patient through a short, 3 mm thick plastic light guide. This 3 mm light pipe was used to both improve electrical isolation and to couple as much light as possible from the mother's abdomen to the silicon detectors. The photodetector electrical outputs travel back through the umbilical cable to the control module where the output from each detector is appropriately processed.

Synchronous detection was used to both reduce extraneous interference from ambient light sources and to improve the signal to noise ratio of the measurements by reducing the contribution of $1/f$ noise. We process the modulated optical signal by first passing the detector output through a high-pass

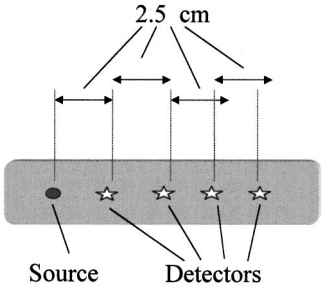

Fig. 10 Optical probe configuration.

filter, and then through a demodulator. The demodulator shifts the 2 kHz signal to a dc level. All other stray light signals exit the detector as frequency-shifted ac signals. The signal-to-noise ratio on the dc level is then improved by reducing the bandwidth with a low-pass filter. However, the bandwidth has to be large enough not to suppress the fetal signal. The bandwidth of our filter was 16 Hz. The four amplified and filtered dc outputs then pass from the control module to the computer for digital acquisition. The signals are digitized at a constant rate and stored in memory. The fetal heart rate was simultaneously monitored with a maternal *trans*-abdominal Doppler probe from a cardiotocograph recorder. Fetal depth was determined by ultrasound just before and after the optical measurements.

7.2 Preliminary Results

We performed experiments on 17 patients. The preliminary results indicate the feasibility for *trans*-abdominal fetus pulse oximetry. Figure 11 illustrates the data collected before and after performing the Fourier transform. The optical signals were slightly modulated by the heart as the elastic vessels expanded and then relaxed with each ventricular contraction. The momentary increase in blood volume increased the light absorption. The detected light signal thus exhibits a slight amplitude modulation in the general shape of a sawtooth [see Figure 11(a)]: a sharp drop in signal corresponding to the ventricular contraction, followed by a slower return as the blood emptied through the capillaries on its way back to the

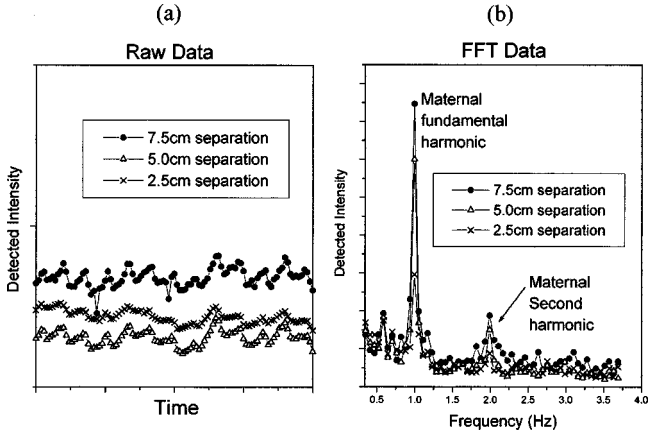

Fig. 11 Data collected (a) before and (b) after performing Fourier transform. No fetal signal is present.

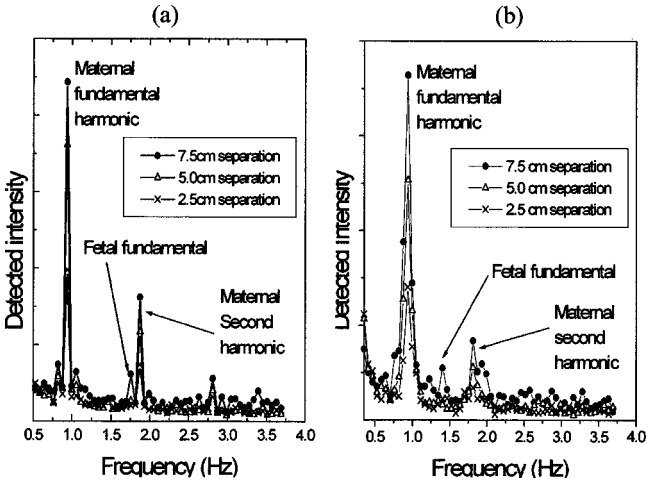

Fig. 12 Data indicating fetal signal along with the maternal signal. (a),(b) Data from two different subjects.

heart. The peaks on the Fourier transformed data [Figure 11(b)] represent the fundamental and first harmonics of the patient's heart.

Since the fetal pulse is generally faster than the maternal pulse, the respective contributions to the optical signals should appear as separate peaks in the Fourier transform. Figures 12(a) and 12(b) demonstrate that we can observe the fetal heart rate and discriminate it from the mother's. The depth of the fetal head from the surface of the mother's abdomen for this particular case was 2.2 cm. Specifically, the fetal heart rate lies between the fundamental and second harmonic of the maternal heart rate. The fetal heart rate was simultaneously monitored by CTG and echography. For this particular case the CTG readings of fetal heart rate were between 80 and 90 beats per minute. This agrees with the peak of ~1.4 Hz indicated in Figure 12. Please note that in this particular case the fetal heart rate is a bit slower than typical fetal heart rate values.

We found that there was a correlation between the detected signal and the depth of the fetus from the surface of the mother's abdomen (determined by ultrasound). When the fetal depth was more than 3.5 cm, the fetal signal detected was weak and difficult to interpret. The signal improved as the depth decreased.

All measurements were performed for three different probe positions, illustrated in Figure 13, to investigate the dependence of probe position relative to fetal position. For the case when the probe was placed on the left side of the mother's abdomen with the source far to the left of the fetal head, we

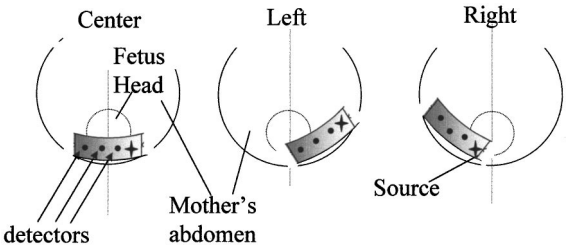

Fig. 13 Three different probe positions on the mother's abdomen.

Table 4 Signal-to-noise ratio dependence on the probe and fetus position.

Total No. of subjects (patients)=17				
		Signal strength (best case per patient)		
		S/N≥2 (good results)	S/N<2 (not bad results)	S/N=0 (no signal)
Overall		5 patients	6 patients	6 patients
Depth of the fetal head from the mother's skin	<1.8 cm	20% (1)	33% (2)	17% (1)
	1.8–3 cm	60% (3)	50% (3)	33% (2)
	>3 cm	20% (1)	17% (1)	50% (3)

were unable to detect the fetal signal. For the two other cases, the center and right probe positions, the fetal signal was easily detected. The summary of the results is presented in Tables 4–7.

Table 4 shows that when the depth of the fetal head was greater than 3 cm the SNR was less than 2 in 50% of the patients. This occurs because the detected light is unable to penetrate these depths. The best results were obtained at depths between 1.8 and 2.5 cm in 60% of the patient data indicating a SNR greater than 2. As one can see from Table 4 there is a decrease in the signal to noise ratio for depths below 1.8 cm. This result needs to be further investigated with photon migration simulations. Presumably, this may be due to the fact that the fetal head is more absorbing than the intermediate maternal tissue or the confounding effects of the amniotic fluid.

Table 5 summarizes the dependence of our measurements on the frequency difference in fetal fundamental and maternal second harmonics. The peaks are easy to discriminate when the frequency difference is greater than 0.1 Hz. The peaks are more difficult to resolve for smaller frequency differences because of peak overlap.

The localization experiments revealed (Table 6) that the best positioning of the probe on the mother's abdomen was on the right side (see Figure 13), or in the center. Left positioning of the probe generally did not produce a signal above the noise floor. This is most likely a result of the large distance between the source and fetus, and thus the fetal pulse contributed weakly to the optical signal. For the center and right probe positions, however, the light source was near the fetal head and thus the fetal pulse had a stronger contribution to the optical signal. In other words, when the source was close to the fetal head, a large fraction of the detected signal had actually sampled the fetus.

The dependence of the detected light intensity on the source/detector separation for three different depth ranges is given in Table 7. As one can see, the best results are obtained for fetal depth of 1.8–3 cm at all three source/detector separations. The signal strength decreased with fetal depth less than 1.8 or more than 3 cm. The signal was too weak at a 10 cm source–detector separation.

With these preliminary results, which demonstrated the possibility of obtaining a fetal signal through the mother's abdomen, our next step will be testing the second dual-wavelength instrument. This would give us the capability to extract the oxygen saturation values from the fetal signals obtained.

Table 5 Signal dependence on frequency difference in fetal fundamental and maternal second harmonics.

Total No. of subjects (patients)=17				
		Signal strength (best case per patient)		
		S/N≥2 (good results)	S/N<2 (not bad results)	S/N=0 (no signal)
Overall		5 patients	6 patients	6 patients
Difference in maternal and fetal heart rates	$\Delta f > 0.1$ Hz	60% (3)	66.6% (4)	16.6% (1)
	$0.005 < \Delta f < 0.1$ Hz	20% (1)	16.6% (1)	16.6% (1)
	$\Delta f < 0.005$	20% (1)	16.6% (1)	66.6% (4)

Table 6 Signal correlation with position of the probe on the mother's abdomen.

Probe position	S/N≥2 (good results)	S/N<2 (not bad results)	S/N=0 (no signal)
Left (No. of patients=17)	12% (2 patients)	12% (2)	76% (13)
Center (No. of patients=17)	59% (10)	29% (5)	12% (2)
Right (No. of patients=17)	70% (12)	18% (3)	12% (2)

Table 7 Signal dependence on the source/detector separation.

Fetal depth S/D separation	<1.8 cm	1.8–3 cm	>3 cm
2.5	S/N<2	S/N≥2	S/N≪2
5.0	S/N<2	S/N≥2	S/N<2
7.5	S/N≪2	S/N<2	S/N<2
10	S/N=0	S/N=0	S/N=0

8 Summary

We have demonstrated that *trans*-abdominal fetal pulse oximetry may be feasible. We discussed the limitations of this technique and factors affecting its accuracy. We theoretically analyzed the optimal wavelength selection for pulse oximetry in general (fetal pulse oximetry in particular, although there is no difference for optimal wavelength selection). This analysis led us to choose a wavelength pair which resulted in the minimum error in saturation: 675–700 and 850–900 nm. During this analysis we took into account the dependence of the photometric error in our wavelength measurement, which has not been done before.

We discussed shunting of the optical signal during the *trans*-abdominal measurement, through the maternal tissue. To evaluate the shunt problem we ran simulations, which indicated that at larger source/detector separations the fraction of the signal reaching the fetus dominates the shunting fraction of light, and therefore using the more distant detector reading for fetal pulse oximetry measurements will reduce the error in the measurement caused by shunting. In addition, we saw that, even though measurement errors at one wavelength can be significant, using ratios of measurements at different wavelengths reduces this error.

Future work includes obtaining data at two wavelengths, which would then give the capability of calculating the fetal oxygen saturation.

Acknowledgments

The authors thank Gargi Vishnoi and Regina Choe for their assistance in collecting the clinical data. They appreciate comments received from Paul Mannheimer and Joe Schmitt, which led to the study of the optical shunt. They would like to express their gratitude to one of the authors (B.C.) for making this project possible. The authors acknowledge support from ODI Grant No. 1R43HL61057-01. One author (D.A.B.) acknowledges additional support from NIH Grant No. R29NS37053.

References

1. J. F. Kelleher, ''Pulse oximetry,'' *J. Clin. Monit* **5**, 37–62 (1989).
2. K. K. Tremper and S. J. Barker, ''Pulse oximetry,'' *Anesthesiology* **70**, 98–108 (1989).
3. G. A. Dildy, S. L. Clark, and C. A. Loucks, ''Preliminary experience with intrapartum fetal pulse oximetry in humans,'' *Obstet. Gynecol. (N.Y.)* **81**, 630–635 (1993).
4. H. McNamara and N. Johnson, ''The effect of uterine contractions on fetal oxygen saturation,'' *Br. J. Obstet. Gynecol.* **102**, 644–647 (1995).
5. G. A. Dildy, P. van den Berg, M. Katz, S. L. Clark, H. W. Jongsma, J. G. Nijhuis, and C. A. Loucks, ''Intrapartum fetal pulse oximetry: Fetal oxygen saturation trends during labor and relation to delivery outcome,'' *Am. J. Obstet. Gynecol.* **171**, 179–184 (1994).
6. J. F. Peterson, ''The development of pulse oximetry,'' *Science* **232**, G135–G140 (1986).
7. J. M. Schmitt, ''Simple photon diffusion analysis of the effects of multiple scattering on pulse oximetry,'' *IEEE Trans. Biomed. Eng.* **38**, 1194–1203 (1991).
8. D. R. Marble, D. H. Burns, and P. W. Cheung, ''Diffusion-based model for pulse oximetry: *In-vivo* and *in-vitro* comparisons,'' *Appl. Opt.* **33**, 1279–1285 (1994).
9. Y. Mendelson and B. D. Ochs, ''Noninvasive pulse oximetry utilizing skin reflectance photoplethysmography,'' *IEEE Trans. Biomed. Eng.* **35**, 798–805 (1988).
10. N. Johnson, V. A. Johnson, J. Fisher, B. Jobbinngs, J. Bannister, and R. J. Lilford, ''Fetal monitoring with pulse oximetry,'' *Br. J. Obstet. Gynaecol.* **98**, 36–41 (1991).
11. H. McNamara, D. C. Chung, R. Lilford, and N. Johnson, ''Do fetal pulse oximetry readings correlate with cord blood oxygenation and acidemia?'' *Br. J. Obstet. Gynaecol.* **99**, 735–738 (1992).
12. H. McNamara, N. Johnson, and R. Lilford, ''The effect on fetal arteriolar oxygen-saturation resulting from giving oxygen to the mother measured by pulse oximetry,'' *Br. J. Obstet. Gynaecol.* **100**, 446–449 (1993).
13. N. Ramanujam and B. Chance, ''Feasibility of measuring fetal cerebral blood oxygenation and volume in utero using trans-abdominal near infrared spectroscopy,'' *Proc. SPIE* **3597**, 661–668, January (1999).
14. F. C. Battaglia and G. Meschia, *An Introduction to Fetal Physiology*, Academic, Orlando (1986).
15. M. Cope, *The Development of a Near-Infrared Spectroscopy System and its Application for Noninvasive Monitoring of Cerebral Blood and Tissue Oxygenation in the Newborn Infant*, University College London, London (1991).
16. S. R. Arridge, ''Optical tomography in medical imaging,'' *Inverse Probl.* **15**, R41–R93 (1999).
17. K. Kramer, *Klin. Wochenschr.* **13**, 379–389 (1934).
18. K. Matthes, *Arch. Exp. Path. Pharmocol.* **179**, 6998–7011 (1935).
19. K. Matthes and F. Gross, *Arch. Exp. Path. Pharmocol.* **191**, 369–379 (1939).
20. P. D. Mannheimer, J. R. Casciani, M. E. Fein, and S. L. Nierlich, ''Wavelength selection for low-saturation pulse oximetry,'' *IEEE Trans. Biomed. Eng.* **44**, 148–156 (1997).

21. M. H. Smith, ''Optimum wavelength combinations for retinal vessel oximetry,'' *Appl. Opt.* **38**, 258–267 (1999).
22. I. S. Saidi, S. L. Jacques, and F. K. Tittel, ''Mie and Rayleigh modeling of visible-light scattering in neonatal skin,'' *Appl. Opt.* **34**, 7410–7418 (1995).
23. R. C. Haskell, L. O. Svaasand, T. Tsay, T. Feng, M. S. McAdams, and B. J. Tromberg, ''Boundary conditions for the diffusion equation in radiative transfer,'' *J. Opt. Soc. Am. A* **11**, 2727–2741 (1994).
24. O. W. van Assendelft, A. Buursma, and W. G. Zijlstra, ''Stability of haemiglobincyanide standards,'' *J. Clin. Pathol.* **49**, 275–277 (1996).
25. S. L. Jacques and L. Wang, ''Monte Carlo modeling of light transport in tissues,'' in *Optical-Thermal Response of Laser-Irradiated Tissue*, Welch and von Gemert, Eds., Plenum, New York, pp. 73–100 (1995).
26. X. Cheng and D. A. Boas, ''Systematic diffuse optical image errors resulting from uncertainty in the background optical properties,'' *Opt. Express* **4**, 299–307 (1999).